Andreas Mischok, Robert Brückner, Hartmut Fröb, Vadim G. Lyssenko, Karl Leo

Photonic lattices in organic microcavities: Bloch states and control of lasing

Erstveröffentlichung in / First published in:

SPIE Organic Photonics + Electronics. San Diego, 2015. Bellingham: SPIE, Vol. 9566 *[Zugriff am: 23.05.2019]*.

DOI: https://doi.org/10.1117/12.2186762

PROCEEDINGS OF SPIE

SPIEDigitalLibrary.org/conference-proceedings-of-spie

Photonic lattices in organic microcavities: Bloch states and control of lasing

Andreas Mischok, Robert Brückner, Hartmut Fröb, Vadim G. Lyssenko, Karl Leo

Andreas Mischok, Robert Brückner, Hartmut Fröb, Vadim G. Lyssenko, Karl Leo, "Photonic lattices in organic microcavities: Bloch states and control of lasing," Proc. SPIE 9566, Organic Light Emitting Materials and Devices XIX, 95660T (22 September 2015); doi: 10.1117/12.2186762

SPIE.

Event: SPIE Organic Photonics + Electronics, 2015, San Diego, California, United States

Photonic lattices in organic microcavities: Bloch states and control of lasing

Andreas Mischok, Robert Brückner, Hartmut Fröb, Vadim G. Lyssenko, and Karl Leo

Institut für Angewandte Photophysik, Technische Universität Dresden, George-Bähr-Strasse 1, D-01069 Dresden, Germany

ABSTRACT

Organic microcavities comprising the host:guest emitter system Alq_3:DCM offer an interesting playground to experimentally study the dispersion characteristics of laterally patterned microlasers due to the broad emission spectrum and large oscillator strength of the organic dye. By structuring of metallic or dielectric sublayers directly on top of the bottom mirror, we precisely manipulate the mode structure and influence the coherent emission properties of the device. Embedding silver layers into a microcavity leads to an interaction of the optical cavity-state in the organic layer and the neighboring metal which red-shifts the cavity resonance, creating a Tamm-plasmon-polariton state. A patterning of the metal can in turn be exploited to fabricate deep photonic wells of micron-size, efficiently confining light in lateral direction. In periodic arrays of silver wires, we create a Kronig-Penney-like optical potential in the cavity and in turn observe optical Bloch states spanning over several photonic wires. We modify the Kronig-Penney theory to analytically describe the full far-field emission dispersion of our cavities and show the emergence of either zero- , π-, or 2π- phase-locking in the system. By investigating periodic SiO_2 patterns, we experimentally observe stimulated emission from the ground and different excited discrete states at room temperature and are able to directly control the laser emission from both extended and confined modes of the photonic wires at room-temperature.

Keywords: Organic Microcavity, Tamm-Plasmon-Polariton, Photonic Lattice, Optical Bloch State, Photon Confinement, Control of Lasing, zero/pi State, Kronig-Penney

1. INTRODUCTION

Microcavity (MC) lasers provide strong vertical confinement of light due to typically very high reflectivities of distributed Bragg reflectors (DBRs) encasing an active cavity layer providing optical net gain to the system.[1] Typical semiconductor cavities include GaAs-based DBRs with active quantum wells and dots,[2] but a large number of active systems have developed, including organic[3] and biological[4] materials. Often, such resonators are planar, exhibiting a parabolic photon dispersion normal to the cavity surface. Micropillars[5] or photonic wires[6,7] are etched from such planar systems to provide stronger confinement and mode control in the lateral direction. Other ways of patterning include the deposition of metal stripes on top of the device[8] or the use of surface acoustic waves,[9] typically producing a weak modulation of the cavity potential. Photonix boxes[10–13] and wires,[14,15] and arrays of these are investigated regarding their confining properties and exhibit more complex mode dispersions. More recently, the ability to strongly couple excitons to cavity polaritons, usually at Helium-temperature, has led to an increasing number of experiments on such systems, including polariton condensation in electrically driven devices.[16] Organic media also have been utilized to facilitate strongly coupled systems and are able to condense even at room-temperature.[17,18]

Interestingly, large coherence lengths in microcavity systems allow the investigation of the formation of photonic bands in various photonic crystal structures patterned into the device. Periodic photonic wires[19] are investigated as well as square-[20–22] or hexagonal[23] lattices leading to clear band structures as commonly observed in solid-state physics. Typically, a weak modulation of the cavity facilitates the formation of extended bands, while deep potentials lead to mode localization and confinement in lateral direction. More recently, we have shown the coexistence of localized and extended states in arrays of photonic wires by introducing thin metal

Send correspondence to A.M. E-mail: andreas.mischok@iapp.de, Telephone: +49 351 463 39189

Organic Light Emitting Materials and Devices XIX, edited by Franky So, Proc. of SPIE Vol. 9566, 95660T
 · doi: 10.1117/12.2186762

stripes into an organic microcavity.[24,25] Here, the thin metal layer leads to the formation of Tamm-plasmon-polariton (TPP) states,[26–28] creating a deep confinement that lies energetically below the cavity resonance. Above the resonance, an array of micron-size wires facilitates the formation of Bloch-like supermodes clearly showing photonic bands separated by corresponding bandgaps.

In this work, we aim to investigate two conceptually different ways to laterally pattern the cavity dispersion - the use of TPPs on the one hand, and an index-guided confinement in dielectric wires on the other hand. While both types prove to be suitable for creating an extended Bloch-like dispersion, we observe differences in the lasing properties of the devices, leading to different possible applications. We describe the dispersion utilizing a modified Kronig-Penney model in good agreement with the experimental observations explaining both localized and extended parts of the Bloch-like states. Both patternings provide a way to directly engineer the optical modes in a microcavity system and lead to a direct way to shape photon and polariton dispersion as well as opening up the possibility to precisely control the build-up of coherence of those particles.

2. SAMPLE AND EXPERIMENTAL SETUP

2.1 Sample and Fabrication

In this work, we experimentally investigate MCs made of highly reflecting ($R \geq 99.5\%$) distributed Bragg reflectors (DBRs) with a design wavelength around 630 nm, providing quality factors on the order of Q=1000. The $\lambda_C/2$ cavity layer is encased by two mirrors and comprises 2wt% of the laser dye Dicyanomethylene-2-methyl-6-p-dimethylaminostyryl-4H-pyran (DCM) doped into the matrix Tris-(8-hydroxyquinolinato)-aluminium (Alq_3, $n_O \approx 1.7$). Apart from the vertical confinement caused by the DBRs, an additional lateral confinement is introduced via several different interlayers, located between bottom DBR and organic cavity layer. By producing stripes of either silver or SiO_2 of few tens of nanometer thickness and micron-scale width, an efficient lateral trapping and modulation of the cavity dispersion can be achieved by spectrally shifting the emission to lower energies.

The DBRs are fabricated by reactive electron beam evaporation of 21 alternating layers of TiO_2 and SiO_2 with quarter-wavelength thicknesses, under a base pressure of 5×10^{-7} mbar and a partial oxygen pressure of 2×10^{-4} mbar. On top of the bottom DBR, the patterned interlayer is produced by two types of photolithography. For metal layers, an etching process is feasible to use, as depicted in Figure 1. A thin metal layer is deposited on the mirror via thermal deposition in vacuum, under a base pressure of 1×10^{-6} mbar. A commercial negative tone photoresist (AZ nLOF2020 by MicroChemicals) of 2 µm thickness is spin-cast on top. After UV-exposure through a chrome contact-mask, the exposed parts of the resist crosslink, while the rest can be dissolved during development in tetramethylammonium hydroxide (TMAH). The remaining resist is further fixed by heating at 120°C for 3 minutes. This patterned resist layer serves as a protection of the underlying silver which can now be etched using either wet-etching in nitric acid (HNO_3), or plasma-etching with Ar ions. Finally, the remaining resist can be removed in various solvents, such as N-methyl-2-pyrrolidone (NMP), leaving the DBR with patterned silver on top for further deposition of the cavity.

As dielectric materials such as SiO_2 are not easily etched, especially without damaging the DBR, a lift-off process is used for them (Fig. 1 (b)). The photoresist is cast directly onto the DBR and, after development, serves as a deposition mask for the SiO_2 layer. After deposition, the resist and SiO_2 on top of it can be lifted off in appropriate solvents. As this step is less controllable and prone to errors, lift-off processes are not used for the metal layer. To improve the lift-off, a double resist system with a fluoropolymer layer as bottom resist can be used,[29] which is soluable in hydrofluoroethers (HFEs,[30]). After lift-off, we obtain a DBR with patterned SiO_2 layer for further use.

On top of the patterned DBRs, the active Alq_3:DCM layer is deposited by thermal co-evaporation at a base pressure of 5×10^{-7} mbar. The sample is finished by depositing the top DBR. In the finished samples (Fig. 1 (a2) and (b2)), the regions of Ag or SiO_2 lead to a redshift of the cavity potential, albeit for different physical reasons.

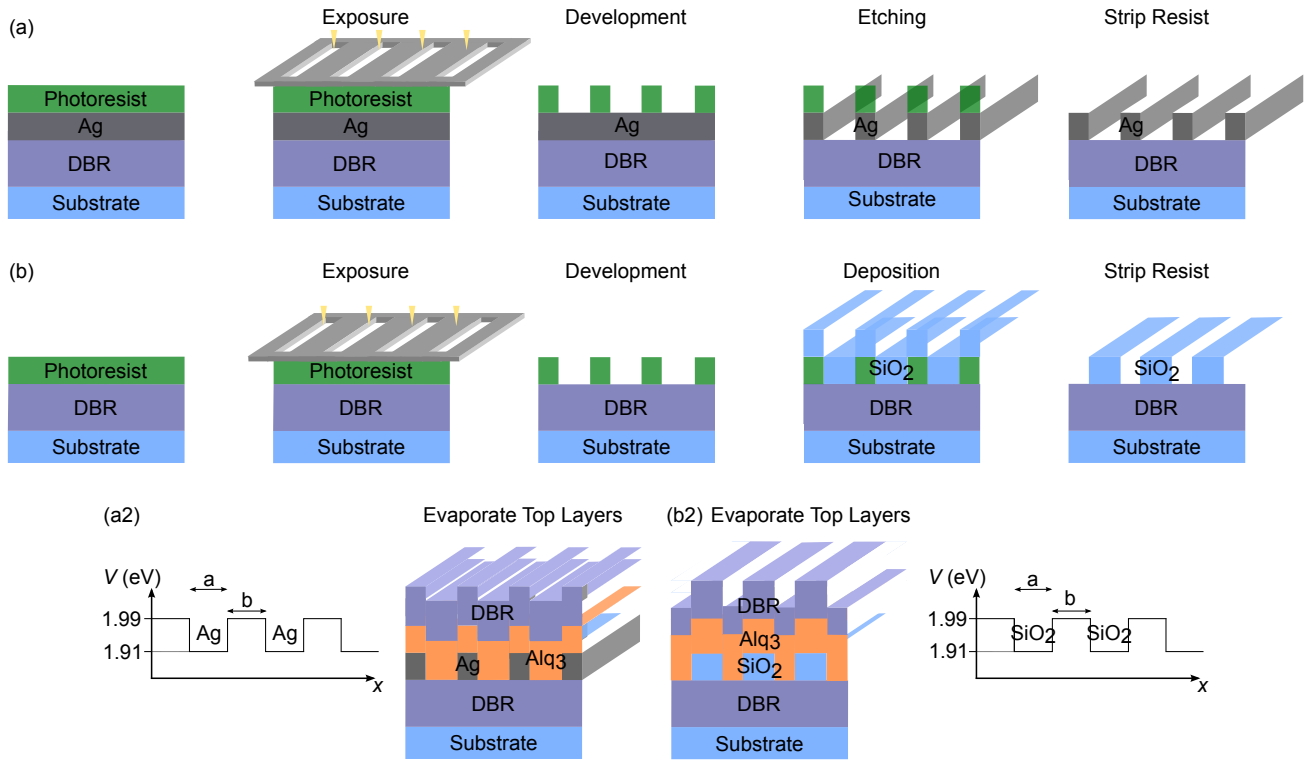

Figure 1. Microcavity fabrication. (a) Photolithographic etching process used for metal layers. After deposition of a bottom DBR and a thin metal layer, a photoresist layer is deposited on top via spin-casting and exposed by i-line UV light (365 nm) through a contact shadow mask. After development, the resist serves as a protection for the underlying metal during the etching process (either wet-etching using HNO_3 or e.g. plasma-etching). After removal of the remaining photoresist, the sample can be finished with the organic and top DBR layers. (a2) Finished sample and resulting photonic potential scheme for the etching process. The formation of Tamm-plasmon-polaritons leads to a redshift of the cavity resonance. (b) Photolithographic lift-off process. Here, the resist is deposited on the DBR itself and, after exposure and development, serves as a lift-off resist for material deposited on top. As e.g. SiO_2 can not be etched without destroying the underlying DBR, this method is favored here. The resulting image will be the negative compared to process (a). (b2) Finished sample and resulting photonic potential scheme for the lift-off process. The increased cavity thickness of the low-index SiO_2 leads to a redshift of the cavity resonance.

2.2 Microphotoluminescence Setup

For below and above threshold investigations of our microcavities, we use either a 405 nm cw laser diode, or a pulsed 532 nm solid state laser (1.5 ns pulse length @ 2 kHz, (a)). In our measurement setup in Figure 2, they are focused onto the sample (d) in spot diameters from 2 µm to several tens of µm to observe photoluminescence (PL) and lasing of the organic microcavity. Using either the near-field or the far-field lens (g), we get access to the spatially or angularly resolved spectrum, respectively, by focusing either the image plane or its Fourier-distribution[8] onto the entrance slit of a 0.6 m imaging spectrometer recorded by a cooled charge-coupled device (CCD) camera (h). The spectra are recorded unpolarized or in different polarizations using the filter (f). The excitation intensity can be tuned via a neutral density filter wheel (b). All experiments are performed at room-temperature under ambient conditions.

3. RESULTS

3.1 Creating the Photon Energy Landscape

In standard microcavities, the position of the resonant mode is either constant over the sample for constant layer thicknesses or continuously tunable, when the cavity layer exhibits a wedged shape. Obtaining sharp changes of the cavity resonance on small length-scales requires the use of patterned interlayers that locally affect photons

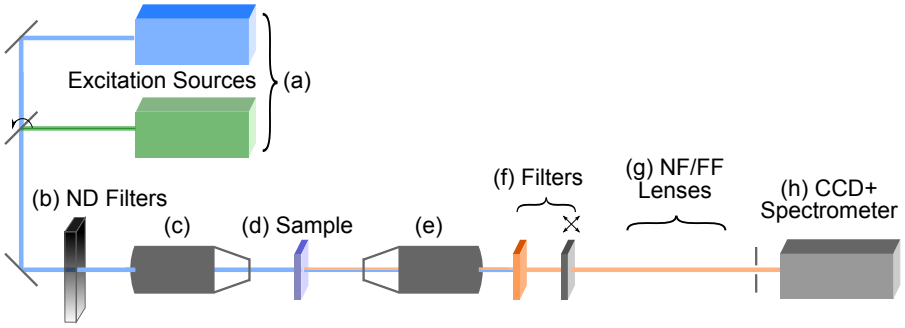

Figure 2. Microphotoluminescence setup. (a) Excitation laser sources. (b) Neutral density filters. (c) Focusing objective 25x, NA=0.5 . (d) Sample. (e) Imaging objective 63x, NA=0.8 . (f) Edge filter for excitation light and polarization analyzer. (g) Near- and far-field lenses. By exchanging one lens by another, we change between a spatially (near-field) and angularly (far-field) resolved image. (h) recording setup switchable by flip-mirror between CCD and spectrometer.

or polaritons either by increasing the optical thickness of the cavity, or by changing their phase at the interface of the layer. Both methods shall be presented in the following.

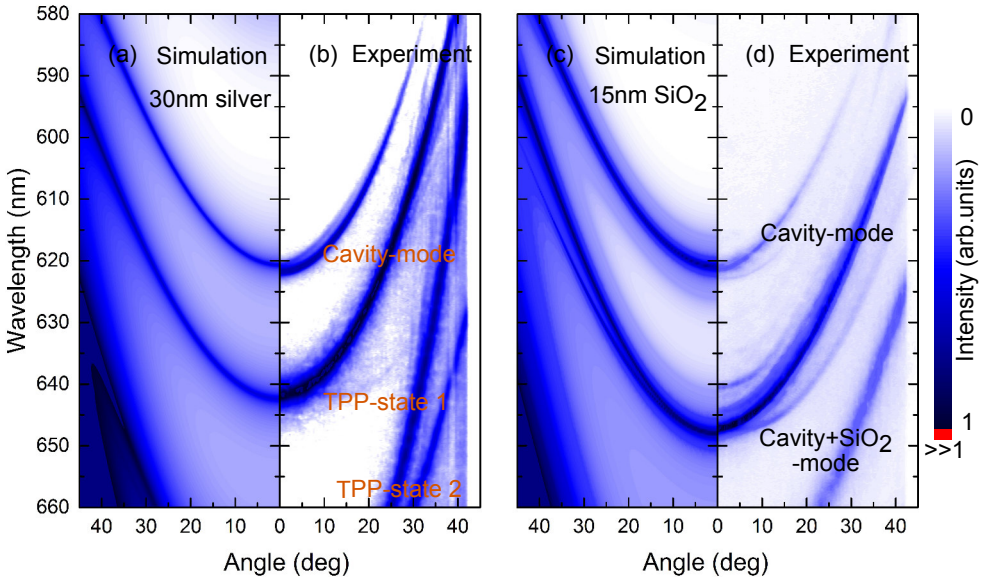

Figure 3. Angle-resolved emission from MC with 30 nm metal ((a) and (b)) and 15 nm SiO_2 ((c) and (d)) interlayers at respective edges of metal/no-metal or SiO_2/no-SiO_2 areas. (a) Simulation of transmission through the metal-cavity. The addition of 30 nm of silver leads to a phase-shift at its interfaces and thus the formation of Tamm-plasmon-polariton (TPP) states at 643 nm (TPP1) and 685 nm (TPP2). The original cavity is visible at 621 nm as both metal and no-metal areas are excited. (b) Corresponding experimental emission spectrum. (c) Simulation of transmission through the SiO_2-cavity. Here, the addition of the thin low-index oxide layer leads to an increase in cavity thickness and thus a shift of the cavity resonance to 649 nm. In contrast to the metal cavity, no phase-change is observed at the SiO_2 interfaces. The original cavity mode is visible at 621 nm, again. (d) Corresponding experimental emission spectrum. Intensity is color-coded in all figures.

Introducing thin silver layers into such a microcavity leads to the formation of Tamm-plasmon-polariton (TPP) states, as the high absorption and vanishing optical thickness of the metal ($n_{Ag} \approx 0.1$) induces a change of phase of photons at the interface to the adjacent layers. Two coupled modes are generated, the TPP state 1, which resides mainly in the organic cavity still, and the TPP state 2, which resides in the first TiO_2 layer of the DBR, next to the silver.[28] Both are red-shifted compared to the original cavity mode - TPP 1 here represents the original cavity state that gradually decreases in energy for thicker metal layers, while TPP 2 emerges from

the red side-band of the DBR and gradually shifts to the blue. At thicknesses >50 nm, the resonances decouple and preserve their spectral distance.[28]

Calculating the spectral position of modes in a metal-organic cavity requires solving the coupled resonator equation:[31]

$$-\frac{t^2}{r^2} = (1-(r_{\mathrm{TiO_2}} r e^{2i\phi_{\mathrm{TiO_2}}})^{-1})(1-(r_{\mathrm{Alq_3}} r e^{2i\phi_{\mathrm{Alq_3}}})^{-1}), \tag{1}$$

where r and t are the reflection and transmission coefficients of the metal layer, $r_{\mathrm{TiO_2}}$ and $r_{\mathrm{Alq_3}}$ the reflection coefficients of the adjacent DBRs on the side of TiO_2 and on the side of the organic active layer. $\phi_{\mathrm{TiO_2}}$ and $\phi_{\mathrm{Alq_3}}$ represent the the phases of propagation through the adjacent layers, respectively. Here, we are interested in the TPP 1 state, which resides mainly in the organic layer and shifts to the red from the initial cavity mode position, for increasing thickness of the silver layer.[28] A full calculation of these properties can be found in[31] by Brückner et al. . The mode positions can then be determined analytically by a transfer matrix algorithm, while for practical purposes a numerically solved algorithm including all 44 layers is used. In our samples, this leads to red-shifts on the order of $V = 69$ meV for 30 nm of silver (compare Fig. 3 (b)) and $V = 75$ meV for 40 nm of silver (compare Figs. 4(a) and 5(a)).

While the redshift in the case of metal interlayers is caused predominantly by the interaction with plasmons and the resulting phase change at the interfaces of the metal layer, a redshift can also be introduced using a non-absorbing low index dielectric interlayer to increase the optical thickness of the cavity. Here, we use SiO_2 as low index material which, even for very low thicknesses, can result in a strong shift of the cavity mode. Assuming no penetration into the DBRs, for cavity modes exactly centered around the stop-band of the mirrors, their energy can easily be calculated:

$$E_{\mathrm{Cav}} = \frac{\pi\hbar c}{n_{\mathrm{Alq_3}} d_{\mathrm{Alq_3}} + n_{\mathrm{SiO_2}} d_{\mathrm{SiO_2}}}, \tag{2}$$

where n_i and d_i are the refractive indices and physical thickness of the organic (Alq_3) cavity layer and the SiO_2 wires. In the real case, such assumptions do not always hold, and detuning as well as polarization of light has to be taken into account. A full calculation can be found in Panzarini et al.[32] and, as applied to a photonic wire cavity, by Löchner et al.[33] As the dielectric structuring is based on a direct increase of the cavity thickness and is thus very efficient, we achieve a redshift of $V = 86$ meV for only 15 nm of SiO_2 between the bottom DBR and the organic cavity layer.

The spectra of half-semi-infinite cavities with either no interlayer, or 30 nm of silver and 15 nm of SiO_2 can be seen in Figure 3. Fig. 3 (a) and (b) show the emission spectra of a microcavity with 30 nm of metal for excitation at the boundary between metal and metal-free area. While the original cavity mode without metal is located at 620 nm and shows the typical parabolic dispersion, in the silver-covered area we see the formation of two TPP states at 643 nm and 685 nm (not shown completely). In (c) and (d) the modes of the SiO_2-cavity are depicted. While the original cavity mode resides at 621 nm, the additional cavity thickness shifts the SiO_2-cavity-state to 649 nm.

Utilizing this red-shifted states in samples patterned on the micron-scale creates strong photonic confinement and, in periodically patterned samples, leads to the formation of photonic Bloch-states exhibiting dispersion relations in analogy to the electronic dispersion in crystal lattices. By creating patterned stripes of 4 µm to 10 µm in width we locally shift the cavity potential by $V > 60$ meV and thus create deep photonic wires with a high number of localized states below the potential barrier. Figure 4 shows the spatially resolved emission from such photonic wires for either TPP-based (a) or dielectric (b) confinement.

In Fig. 4 (a), we observe a strong spatial confinement of photons in the spectral range between 658 nm to 685 nm at the position of the 40 nm-thick metal layer. The emission from photonic wires is discretized in energy and exhibits modes of increasing number of antinodes that are directly observable in the emission of our sample. As only discrete k-values are allowed inside the well, the energies (at $k_y = 0$) are qualitatively given by:[10]

$$E_m = \hbar c\sqrt{k_z^2 + k_y^2 + k_z^2} = \hbar c\sqrt{k_z^2 + \frac{(m+1)^2\pi}{n_{\mathrm{C}}^2 a^2}} = \pi\hbar c\sqrt{\frac{1}{(n_{\mathrm{C}} L_{\mathrm{C}})^2} + \frac{(m+1)^2}{n_{\mathrm{C}}^2 a^2}}, \tag{3}$$

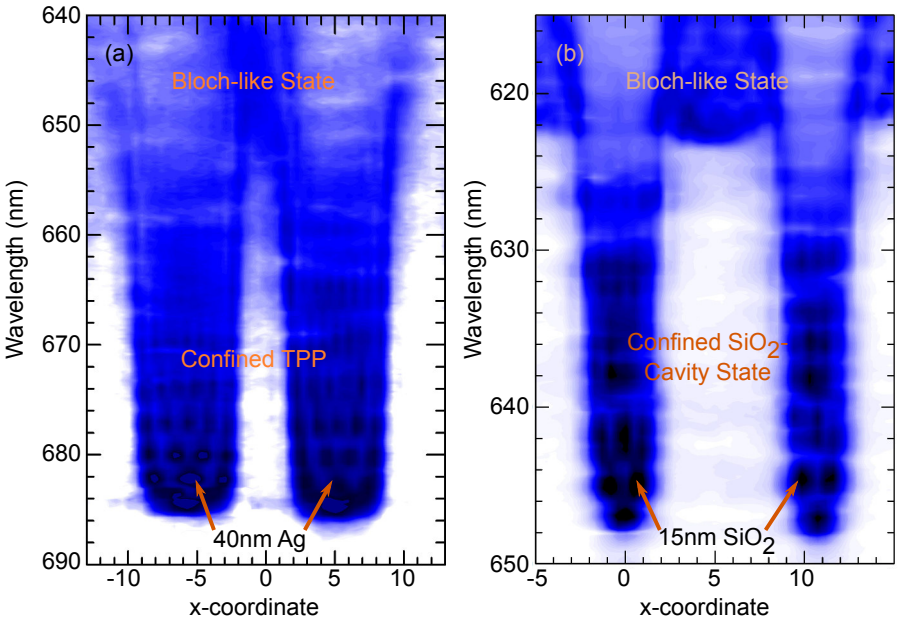

Figure 4. (a) Spatially resolved emission spectrum of a MC with 40 nm-thick metal stripes of ≈7 µm in width. In the range of 658 nm - 685 nm, confined Tamm-plasmon-polaritons are visible as discrete standing waves with an increasing number of antinodes due to the strong confinement below the barrier. Above the barrier, an extended Bloch-like state becomes visible. (b) Spatially resolved emission spectrum of a MC with SiO_2 stripes of ≈4.5 µm in width. Here, confined states are visible in the range of 649 nm - 622 nm. Despite their different physical origins, both types of structuring produce similar strong lateral confinement.

where n_C and L_C are the effective cavity refractive index and thickness, which has to be adapted to the phase change at the metal interface, accordingly, and c is the speed of light in vacuum. The index m describes the number of confined state from ground (m=0) to highest excited state below the barrier. Above the barrier (< 658 nm), extended states fill the spectrum.

Similarly strong confinement can be observed in SiO_2 stripes, where a comparably small physical thickness of only 15 nm is enough to create the deep potential of the photonic wire from 621 nm to 649 nm. In 4.5 µm thick wires, we again observe a discretization of modes below the barrier. The calculation of their energy levels follows Equation (3) again, where the cavity thickness $n_C L_C$ is directly calculated from the optical thicknesses of organic and SiO_2 layers $n_{Alq_3} L_{Alq_3} + n_{SiO_2} L_{SiO_2}$. The smaller width of the wire here leads to a larger spacing between discrete states. In addition, a detuning of this particular cavity with respect to the DBR design wavelength facilitates a splitting of each discrete mode into its respective polarization directions TE and TM, where TE modes lie lower in energy than their TM counterparts. A full calculation of these polarization-dependent mode positions requires a full consideration of the penetration of modes into adjacent DBR layers[32,33] and shall not be given here.

The types of structuring employed here serve similarly well to confine light inside of microcavities, even though the physics behind the shift of the photonic potential is completely different. Both, plasmonic and index-guided confinement, may be utilized to shape photon or polariton dispersions towards interesting new experiments.

3.2 Photonic Bloch States in Metal- or SiO_2-Patterned Cavities

While the spatially-resolved near field gives a good representation of the photonic well and its corresponding modes and a direct observation of the photonic potential, the full observation of Bloch-states can only be made in angle-resolved emission spectra. Figure 5 shows the dispersion for both metal- (a) and SiO_2 (c) cavities below and above their potential barrier. Below the barrier, the discrete states exhibit a flat dispersion and $(m-1)$ submaxima inside the typical cavity parabola, according to the index m of discrete state. While even states

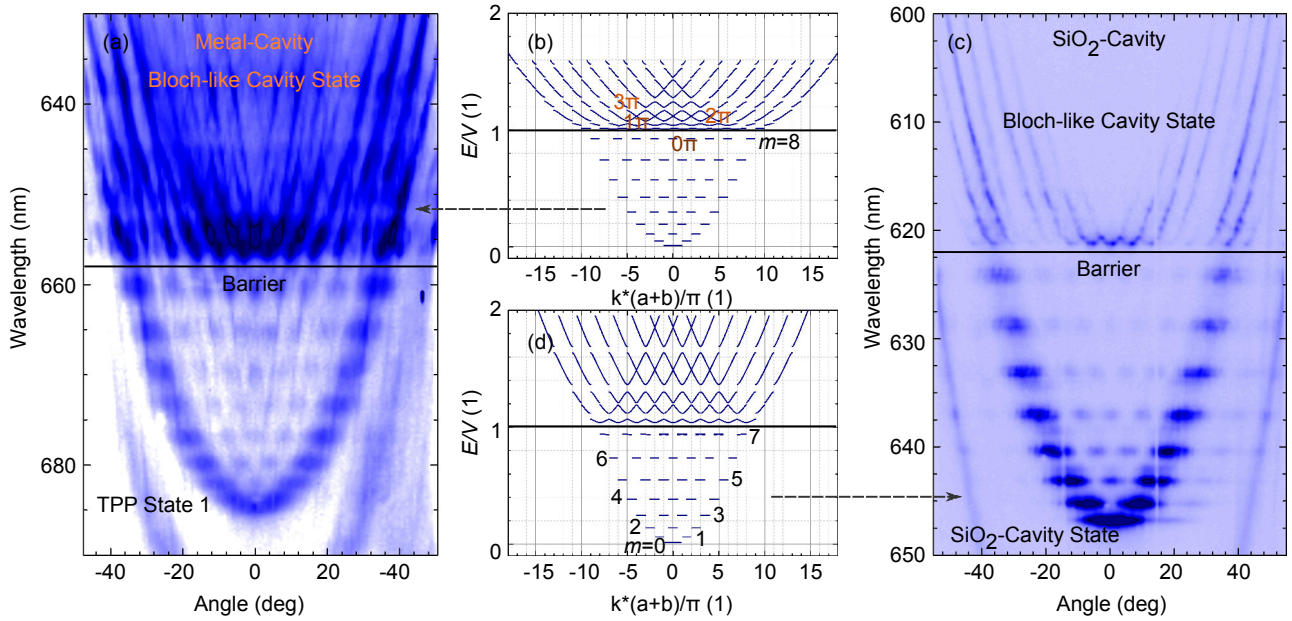

Figure 5. Spontaneous emission spectra from laterally patterned microcavities. (a) Angle-resolved emission spectrum of a MC with a 40 nm-thick silver layer of ≈4 µm in width. Below the barrier at 658 nm, discrete TPP states are confined within the metal stripe, exhibiting a flat dispersion. Above the barrier, an extended Bloch-like spectrum becomes visible. (b) Kronig-Penney calculation for (a) with Bragg-scattering up to the eighth order. (c) Angle-resolved emission spectrum of a MC with a 15 nm thick SiO_2 layer of ≈4.5 µm in width. Again, a discrete, confined spectrum becomes visible below the barrier, albeit of higher quality owing to the low absorption of SiO_2 in comparison to silver. Above the barrier, a similar Bloch-like bandstructure with clear bandgaps is visible. (d) Kronig-Penney calculation for (c) with Bragg-scattering up to the eighth order.

($m = 0, 2, ...$) exhibit always an antinode in the center, odd states ($m = 1, 3, ...$) show the first antinodes at $k = \pi/(a + b)$ and thus show no emission in normal direction to the sample surface.

Above the barrier, the formation of photonic energy bands with band-gaps becomes clear in both cases. Here, the lowest above-barrier state starts, complementary to the oddity of the highest below-barrier state, either at $k = 0$ ((c), $m_{\text{below}} = 7$) or at a π-state ((a), $m_{\text{below}} = 8$). As the intensity of light is dampened by the metal layer, the below-barrier states in the metal cavity exhibit a lower intensity than the above-barrier states, while in the SiO_2 cavity a more evenly distributed intensity can be observed. Nevertheless do both types of structuring show not only the formation of localized states below but also a clear and directly accessible Bloch-like dispersion above the photon potential barrier. Furthermore, this interaction between different optical states of several periodic wires at macroscopic distances showcases the large spatial coherence in the system, at room-temperature, even below the lasing threshold.

The formation of Bloch-like optical modes can be calculated using a modified Kronig-Penney model. The cavity dispersion is related to the dispersion of a free electron via:

$$E(k_x) = \sqrt{\left(\frac{\pi\hbar c}{n_c L_c}\right)^2 + \frac{\hbar^2 c^2}{n_c^2} k_x^2} \approx E(0) + \frac{\hbar^2 k_x^2}{2m_x^*}, \tag{4}$$

where the starting energy $E(0)$ can be calculated as above and the photons obtain an effective mass $m_x^* \approx \pi\hbar n_c / c L_c$ on the order of $10^{-5} m_e$ (electron mass). A full consideration of all applicable parameters includes the polarization into the effective mass as shown in detail by Löchner et al.[33]

Utilizing this analogy, the Kronig-Penney model can be computed from the time-independent Schrödinger equation:

$$\begin{aligned} \frac{\partial^2\psi}{\partial x^2} + \frac{2m^*E}{\hbar^2}\psi = 0 \qquad & 0 < x < b \\ \frac{\partial^2\psi}{\partial x^2} + \frac{2m^*(E-V_0)}{\hbar^2}\psi = 0 \qquad & -a < x < 0, \end{aligned} \tag{5}$$

and periodically continued, yielding wave functions:[34]

$$\begin{aligned} \psi_1 &= Ae^{i\alpha x} + Be^{-i\alpha x}; \qquad \text{with} \quad \alpha = \frac{\sqrt{2m_x^*E}}{\hbar} \\ \psi_2 &= Ce^{-i\beta x} + De^{i\beta x}; \qquad \text{with} \quad \beta = \frac{\sqrt{2m_x^*(E-V)}}{\hbar}, \end{aligned} \tag{6}$$

with propagation wavevectors α and β and normalization constants A, B, C, D. Applying the Bloch-theorem and continuity conditions, this set of equations can be solved by computing the determinant of the coefficient matrix, leading to a transcendental equation for the energy dispersion:

$$\frac{\beta^2 - \alpha^2}{2\alpha\beta}\sinh(\beta b)\sin(\alpha a) - \cosh(\beta b)\cos(\alpha a) = \cos((a+b)\times k). \tag{7}$$

This equation can be solved graphically or numerically and directly yields the energy dispersion for photons in periodically patterned microcavities. Figure 5 (b) and (d) show this calculation for the corresponding samples (a) and (c). We obtain an excellent agreement regarding number and positioning of localized states and formation of extended Bloch-like states above the potential barrier. As the emission of microcavities is influenced by Bragg-scattering at the boundaries of the Brillouin zones, we include Bragg-scattered replica up to order 8 in the calculation.

Both types of structuring facilitate an engineering of the cavity dispersion despite fundamentally different physical origins. While coupled Tamm-plasmon states enable interesting insights into the coupling of photons to plasmons and a direct route to electrical excitation, structuring via loss-less dielectric materials provides the highest optical quality of the sample and very narrow modes with high quality factors both in vertical and lateral direction.

3.3 Laser Modes in Periodically Patterned Microcavities

By increasing the excitation intensity, both MCs can be brought to lase at threshold energies on the order of the magnitude of a few nJ/Pulse. The laser mode characteristics however differ strongly from planar cavities, where stimulated emission takes place always at the bottom of the cavity parabola, at k=0. There, the apex provides a high density of states (DOS) and therefore an accumulation of field intensity necessary to overcome the lasing threshold. The coherent interaction between states located in different photonic potential wells or on top of the barrier in patterned MCs severely alters the photon dispersion as seen above and provides a concentration of photon DOS $\rho(E) = 2(\mathrm{d}k/\mathrm{d}E)/\pi$[35] next to photonic bandgaps and at discrete states below the barrier. This leads to a manifold increase of possible lasing modes both on top of the structured areas and inbetween. Even though lasing in TPP structures has been reported recently,[27,36] the additional metal absorption even in such TPP states makes lasing of this particular state difficult to observe. Here, the above-barrier extended Bloch states provide the ability to observe unusual lasing modes of the cavity state at non-zero in-plane momentum. Figure 6 (a) depicts a measurement above threshold, showing lasing (in red) from an excited above-barrier state. Here, the laser mode is concentrated at $k = \pm\pi/(a+b)$ and no emission in normal direction is observed. Due to its comparably weaker intensity, the spontaneous emission of the TPP states is not visible here. By further increasing the excitation pulse energy, we observe multimode lasing from up to 4 different modes at increasing $k = \pm m\pi$, shown in Fig. 6 (b).

On the other hand, the almost loss-less SiO_2 wires provide an ideal spot for tunable lasing modes in their discrete states. By engineering the spatial distribution of excitation in the system, different laser modes can be selectively excited.[38] In Fig. 6 (c) and (d), the spatially and angle-resolved spectra of lasing from a high excited

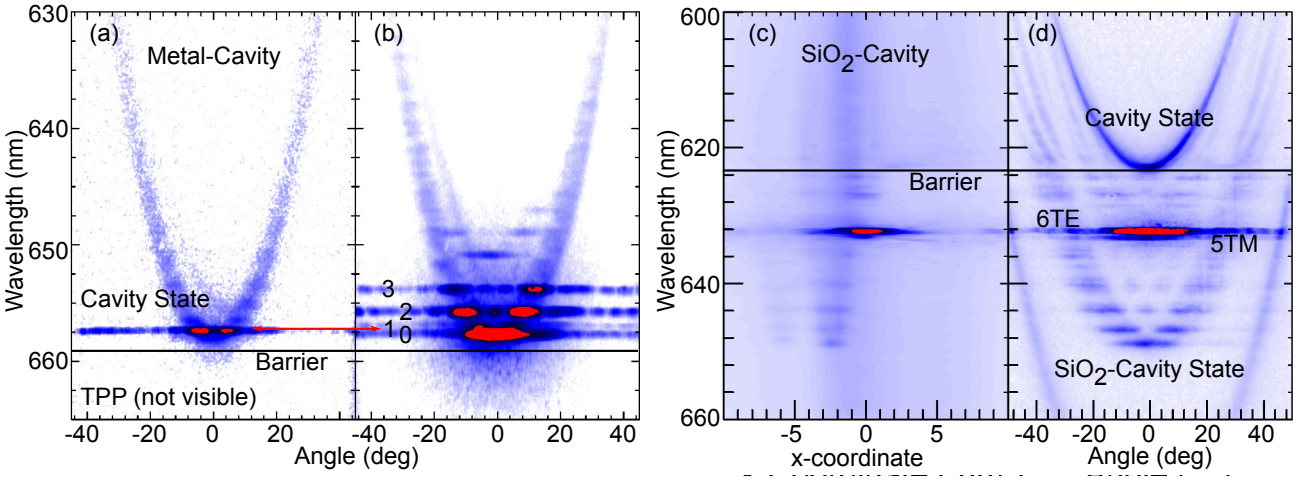

Figure 6. Lasing spectra of patterned MCs. (a) Angle-resolved lasing of the second cavity-state (m=1) in a MC with 40 nm-thick silver stripes of ≈4 µm in width. The lateral patterning enables lasing of non-ground modes in the cavity state at the position of $\pm 1\pi$. (b) Angle-resolved lasing of multiple states in the metal-cavity at $k = m \times \pi$, going up to m=3. (c) Lasing of a highly excited SiO_2-cavity state in a MC with 15 nm SiO_2 of ≈4.5 µm in width. Due to the low absorption of SiO_2 and the flat dispersion provided by the confinement, higher order states can be excited. (d) Angle-resolved image of (c), showing lasing at high m. Due to polarization splitting in this MC, the lasing mode is split into the m=6 TE- and m=5 TM- modes.

discrete state can be seen. Due to polarization splitting,[37] the discrete states split into TE- and TM-polarized modes and the final lasing modes is split into the 6TE and 5TM mode due to their close spatial overlap.

The lateral patterning of microcavities provides an interesting playground for engineering coherent interaction of photons and polaritons at macroscopic distances. While metallic patterning provides coherently coupled states above the potential barrier as well as a direct electrical access for future charge carrier injection, SiO_2 wires provide continously tunable coherent states[38] in their deep photonic potential wells. Such patterning can be integrated into smallest devices on the micron-scale in all dimensions.

4. CONCLUSION

We have presented laterally patterned organic microcavities, where we employ conceptually very different structured interlayers to produce shifts in the cavity potential and facilitate the formation of localized and extended Bloch-like states. In metal-organic MCs, the formation of Tamm-plasmon-polaritons is utilized, enabling the observation of photonic wells, Bloch-states and laser emission at non-zero in-plane momentum, also showcasing their macroscopic coherence at room-temperature. Patterning the cavity using the almost loss-less SiO_2, we observe a potential shift due to an increased cavity thickness and observe Bloch-states of very high optical quality in all directions. Continuously tunable lasing is enabled by exciting different discrete states in the system. The experimental observation of Bloch-states is assisted by a modified Kronig-Penney calculation, giving an analytical model for the complex dispersion in the cavities. Both types of structuring show promising features for shaping photonic and polaritonic states in MCs and controlling the build-up of coherence in those systems.

ACKNOWLEDGEMENTS

We thank Alexander A. Zakhidov for details and assistance on photolithographic structuring and Matthias Böhm for assistance in programming. This work was supported by the German Bundesministerium für Bildung und Forschung through the InnoProfile Project (03IP602) and the Deutsche Forschungsgemeinschaft (DFG projects LE 747/37-1 and LE 747/41-1). A.M. acknowledges support by the European Social Fund via the OrganoMechanics project and the European project NUDEV. Support from the excellence cluster cfaed is gratefully acknowledged.

REFERENCES

[1] Vahala, K. J. "Optical microcavities," *Nature* **424**, 839 (2003).

[2] Yokoyama, H., Nishi, K., Anan, T., Yamada, H., Brorson, S. D., and Ippen, E. P., "Enhanced spontaneous emission from GaAs quantum wells in monolithic microcavities," *Appl. Phys. Lett.* **57**, 2814 (1990).

[3] Kozlov, V. G., Bulovic, V., Burrows, P. E., and Forrest, S. R., "Laser action in organic semiconductor waveguide and double-heterostructure devices," *Nature* **389**, 362 (1997).

[4] Gather, M. C., and Yun, S. H. "Single-cell biological lasers," *Nature Photonics* **5**, 406 (2011).

[5] Reitzenstein, S., Bazhenov, A., Gorbunov, A., Hofmann, C., Münch, S., Löffler, A., Kamp, M., Reithmaier, J. P., Kulakovskii, V. D., and Forchel, A., "Lasing in high-Q quantum-dot micropillar cavities," *Applied Physics Letters* **89**(5), 051107 (2006).

[6] Tanese, D., Flayac, H., Solnyshkov, D., Amo, A., Lemaître, A., Galopin, E., Braive, R., Senellart, P., Sagnes, I., Malpuech, G., and Bloch, J. "Polariton condensation in solitonic gap states in a one-dimensional periodic potential," *Nature Communications* **4**, 1749 (2013).

[7] Constantin, C., Martinet, E., Oberli, D. Y., Kapon, E., Gayral, B., and Gérard, J. M., "Quantum wires in multidimensional microcavities: Effects of photon dimensionality on emission properties," *Phys. Rev. B* **66**, 165306 (2002).

[8] Lai, C. W., Kim, N. Y., Utsunomiya, S., Roumpos, G., Deng, H., Fraser, M. D., Byrnes, T., Recher, P., Kumada, N., Fujisawa, T., and Yamamoto, Y., "Coherent zero-state and pi-state in an exciton-polariton condensate array," *Nature* **450**, 529–U8 (2007).

[9] Cerda-Mèndez, E. A., Sarkar, D., Krizhanovskii, D. N., Gavrilov, S. S., Biermann, K., Skolnick, M. S., and Santos, P. V., "Exciton-Polariton Gap Solitons in Two-Dimensional Lattices," *Phys. Rev. Lett.* **111**, 146401 (2013).

[10] Reithmaier, J. P., Röhner, M., Zull, H. Schäfer, F., Forchel, A., Knipp, P. A., and Reinecke, T. L., "Size Dependence of Confined Optical Modes in Photonic Quantum Dots," *Phys. Rev. Lett.* **78**, 378 (1997).

[11] Mischok, A., Brückner, R., Sudzius, M., Reinhardt, C., Lyssenko, V. G., Fröb, H., and Leo, K., "Photonic confinement in laterally structured metal-organic microcavities," *Appl. Phys. Lett.* **105**, 051108 (2014).

[12] Ferrier, L., Wertz, E., Johne, R., Solnyshkov, D. D., Senellart, P., Sagnes, I., Lemaître, A., Malpuech, G., and Bloch, J., "Interactions in Confined Polariton Condensates," *Phys. Rev. Lett.* **106**, 126401 (2011).

[13] El Daïf, O., Baas, A., Guillet, T., Brantut, J.-P., Idrissi Kaitouni, R., Staehli, J. L., Morier-Genoud, F. and Deveaud, B., "Polariton quantum boxes in semiconductor microcavities," *Appl. Phys. Lett.* **88**, 061105 (2006).

[14] Schmidt-Grund, R., Hilmer, H., Hinkel, A., Sturm, C., Rheinländer, B., Gottschalch, V., Lange, M., Zúñiga Pérez, J., and Grundmann, M., "Two-dimensional confined photonic wire resonators - strong light-matter coupling," *physica status solidi (b)* **247**(6), 1351–1364 (2010).

[15] Mischok, A., Lemke, F., Reinhardt, C., Brückner, R., Zakhidov, A. A., Hintschich, S. I., Fröb, H., Lyssenko, V. G., and Leo, K., "Dispersion tomography of an organic photonic-wire microcavity," *Applied Physics Letters* **103**(18), 183302 (2013).

[16] Schneider, C., Rahimi-Iman, A., Young Kim, N., Fischer, J., Savenko, I. G., Amthor, M., Lermer, M., Wolf, A., Worschech, L., Kulakovskii, V. D., Shelykh, I. A., Kamp, M., Reitzenstein, S., Forchel, A., Yamamoto, Y., and Höfling, S., "An electrically pumped polariton laser," *Nature* **497**, 348 (2013).

[17] Plumhof, J. D., Stöferle, T., Mai, L., Scherf, U., and Mahrt, R. F., "Room-temperature Bose-Einstein condensation of cavity exciton-polaritons in a polymer," *Nature Materials* **13**, 247 (2013).

[18] Daskalakis, K. S., Maier, S. A., Murray, R., and Kèna-Cohen, S. "Nonlinear interactions in an organic polariton condensate," *Nature Materials* **13**, 271 (2014).

[19] Zhang, L., Xie, W., Wang, J., Poddubny, A., Lu, J., Wang, Y., Gu, J., Liu, W., Xu, D., Shen, X., Rubo, Y. G., Altshuler, B. L., Kavokin, A. V., and Chen, Z. "Weak lasing in one-dimensional polariton superlattices," *Proc. Natl Acad. Sci. USA* **112**, E1516 (2015).

[20] Kim, N. Y., Kusudo, K., Wu, C., Masumoto, N., Löffler, A., Höfling, S., Kumada, N., Worschech, L., Forchel, A., and Yamamoto, Y., "Dynamical d-wave condensation of exciton-polaritons in a two-dimensional square-lattice potential," *Nature Phys.* **7**, 681 (2011).

[21] Zhang, B., Brodbeck, S., Wang, Z., Kamp, M., Schneider, C., Höfling, S., and Deng, H., "Coupling polariton quantum boxes in sub-wavelength grating microcavities," *Appl. Phys. Lett.* **106**, 051104 (2015).

[22] Winkler, K., Fischer, J., Schade, A., Amthor, M., Dall, R., Gessler, J., Emmerling, M., Ostrovskaya, E. A., Kamp, M., Schneider, C., and Höfling, S., "A polariton condensate in a photonic crystal potential landscape," *New J. Phys.* **17**, 023001 (2015).

[23] Jacqmin, T., Carusotto, I., Sagnes, I., Abbarchi, M., Solnyshkov, D. D., Malpuech, G., Galopin, E., Lemaître, A., Bloch, J., and Amo, A., "Direct Observation of Dirac Cones and a Flatband in a Honeycomb Lattice for Polaritons," *Phys. Rev. Lett.* **112**, 116402 (2014).

[24] Brückner, R., Zakhidov, A. A., Scholz, R., Sudzius, M., Hintschich, S. I., Froeb, H., Lyssenko, V. G., and Leo, K., "Phase-locked coherent modes in a patterned metal-organic microcavity," *Nature Photonics* **6**, 322–326 (2012).

[25] Mischok, A., Lyssenko, V. G., Brückner, R., Löchner, F., Zakhidov, A. A., Fröb, H., and Leo, K., "Zero- and π-States in a Periodic Array of Deep Photonic Wires," *Adv. Opt. Mater.* **2**(8), 746 (2014).

[26] Kaliteevski, M., Iorsh, I., Brand, S., Abram, R. A., Chamberlain, J. M., Kavokin, A. V., and Shelykh, I. A., "Tamm plasmon-polaritons: Possible electromagnetic states at the interface of a metal and a dielectric Bragg mirror," *Phys. Rev. B* **76**, 165415 (2007).

[27] Symonds, C., Lheureux, G., Hugonin, J. P., Greffet, J. J., Laverdant, J., Brucoli, G., Lemaître, A., Senellart, P., and Bellessa, J., "Confined Tamm Plasmon Lasers," *Nano Letters* **13**(7), 3179 (2013).

[28] Brückner, R., Sudzius, M., Hintschich, S. I., Fröb, H., Lyssenko, V. G., and Leo, K., "Hybrid optical Tamm states in a planar dielectric microcavity," *Phys. Rev. B* **83**, 033405 (2011).

[29] Krotkus, S., Ventsch, F., Kasemann, D., Zakhidov, A.A., Hofmann, S., Leo, K., and Gather, M.C., "Photopatterning of Highly Efficient State-of-the-Art Phosphorescent OLEDs Using Orthogonal Hydrofluoroethers" *Advanced Optical Materials* **2**(11), 1043 (2014).

[30] Zakhidov, A. A., Lee, J.-K., Fong, H. H., DeFranco, J. A., Chatzichristidi, M., Taylor, P. G., Ober, C. K., and Malliaras, G. G., "Hydrofluoroethers as orthogonal solvents for the chemical processing of organic electronic materials," *Advanced Materials* **20**(18), 3481 (2008).

[31] Brückner, R., Sudzius, M., Hintschich, S. I., Fröb, H., Lyssenko, V. G., Kaliteevski, M. A., Iorsh, I., Abram, R. A., Kavokin, A. V., and Leo, K., "Parabolic polarization splitting of tamm states in a metal-organic microcavity, *Applied Physics Letters* **100**(6) (2012).

[32] Panzarini, G., Andreani, L. C., Armitage, A., Baxter, D., Skolnick, M. S., Astratov, V. N., Roberts, J. S., Kavokin, A. V., Vladimirova, M. V., and Kaliteevski, M. A., "Exciton-light coupling in single and coupled semiconductor microcavities: Polariton dispersion and polarization splitting," *Phys. Rev. B* **59**, 5082 (1999).

[33] Löchner, F., Mischok, A., Brückner, R., Zakhidov, A.A., Fröb, H., Lyssenko, V. G., and Leo, K., "Coexisting localized and extended optical Bloch states in a periodic deep wire array microcavity," *Superlattice Microst* DOI:10.1016/j.spmi.2015.06.020 (2015).

[34] Cho, H.-S., and Prucnal, P. R., "New formalism of the Kronig-Penney model with application to superlattices," *Phys. Rev. B* **36**, 3237 (1987).

[35] Wolfe, J. C., "Summary of the Kronig-Penney electron," *Am. J. Phys.* **46**, 1012 (1978).

[36] Brückner, R., Lyssenko, V. G., Hofmann, S., and Leo, K., "Lasing of Tamm states in highly efficient organic devices based on small-molecule organic semiconductors," *Faraday Discuss.* **174**, 183 (2014).

[37] Becker, F., Langner, M., Fröb, H., Lyssenko, V. G., Leo, K., and Adachi, C., "Dependence of polarization splitting on mode tuning in microcavities." *Appl. Phys. Lett.* **95**, 191106 (2009).

[38] Mischok, A., Brückner, R., Zakhidov, A. A., Fröb, H., Lyssenko, V. G., and Leo, K., "Control of Lasing from Bloch-States in Microcavity Photonic Wires via Selective Excitation and Gain," *Phys. Rev. Applied* **3**, 064016 (2015).